Coupled Systems Mechanics, *Vol. 4, No. 3 (2015) 211-235*
DOI: http://dx.doi.org/10.12989/csm.2015.4.3.211

Localized failure in damage dynamics

Xuan Nam Do[1a], Adnan Ibrahimbegovic[*1,2] and Delphine Brancherie[1b]

[1]*Université de Technologie Compiègne / Sorbonne Universités, Laboratoire Roberval de Mécanique Centre de Recherche Royallieu, Rue Personne de Roberval, 60200 Compiègne, France*
[2]*Chair for Computational Mechanics & IUF, France*

(Received May 17, 2015, Revised August 27, 2015, Accepted September 5, 2015)

Abstract. In this work we present a one-dimensional damage model capable of representing the dynamic fracture for elastodamage bar with combined hardening in fracture process zone - FPZ and softening with embedded strong discontinuities. This model is compared with another one we recently introduced (Do *et al*. 2015) and it shows a good agreement between two models. Namely, it is indicated that strain-softening leads to a sensitivity of results on the mesh discretization. Strain tends to localization in a single element which is the smallest possible area in the finite element simulations. The strain-softening element in the middle of the bar undergoes intense deformation. Strain increases with increasing mesh refinement. Strain in elements outside the strain-softening element gradually decreases to zero.

Keywords: dynamics; fracture process zone – FPZ; strain-softening; localization; finite element; embedded discontinuity

1. Introduction

Damage is usually considered as a deformation driven process and standard damage material models are generally based on the continuum damage mechanics (CDM) approach with the pioneering work of Kachanov (1958). CDM represents microscopic heterogeneous damage on the macroscale. Degradation of material properties, which results in behavior known as strain-softening, at the microscale due to nucleation and coalescence of cavities, microcracks, microvoids, and similar defects is described by a loss of effective load carrying area designated with a damage variable. This variable can be scalar or tonsorial. The expressions for constitutive equations are derived from well-known principals, such as effective stress in conjunction with equivalence hypothesis, such as strain equivalence or energy equivalence. However, it is well documented that the boundary value problem in continuum damage models becomes ill-posed during strain-softening, where the stress-strain diagram exhibits a negative slope (Fig. 1), leading to pathological sensitivity of the numerical results to the size of finite elements. The tangent stiffness matrix loses its positive-definiteness in the strain-softening area, as shown rigorously by Bazant (1976). As a consequence, the partial differential equations change their type from

∗Corresponding author, Professor, E-mail: adnan.ibrahimbegovic@utc.fr
[a] E-mail: xuan-nam.do@utc.fr
[b] E-mail: delphine.brancherie@utc.fr.

http://www.techno-press.org/?journal=csm&subpage=7 ISSN: 2234-2184 (Print), 2234-2192 (Online)

hyperbolic to elliptic which does not fit the initial dynamic equation. In this case the CDM approach ceases to be mathematically meaningful. In other words, this kind of approach is not adequate for post-localization studies where strain-softening appears.

In the attempt to overcome the shortcomings of local theories for modelling strain-softening, some alternatives have been proposed. One of the most efficient among them is the embedded discontinuity approach. In this method, the strain or displacement field is enhanced to capture the discontinuity. The early works of Simo *et al*. (1993), Oliver (1996), Wells and Sluys (2000), and Alfaiate *et al*. (2002) provide different representations of the embedded discontinuity method. Most of studies on finite elements with embedded discontinuities only consider quasi-static problems, while dynamic analyses with this approach (e.g., Huespe *et al*. 2006, Armero and Linder 2009) are very rare. As the main novelty, herein we present a discrete bar model in which strain-hardening and strain-softening elastodamage behavior are combined in dynamics. We further compare with analytical solution of Bazant and Belytschko (1985) as well as with our recent work (Do *et al*. 2015) on plasticity models with discontinuity, thus providing an alternative strong discontinuity approach to modeling failure phenomena in dynamics.

The paper is organized as follows: Section 2 is devoted to the theoretical formulation. In Section 3, we revisit a closed-form reference solution for a dynamic strain-softening problem without FPZ, followed by Section 4 with the numerical implementation for one-dimensional bar with embedded strong discontinuities. Section 5 will carry out numerical simulations and give comparison between this model and another one we recently introduced. Finally, conclusions are presented in Section 6.

2. Theoretical formulation

2.1 Elastodamage part

2.1.1 Model summary

The basic development for the 1D hardening part results with

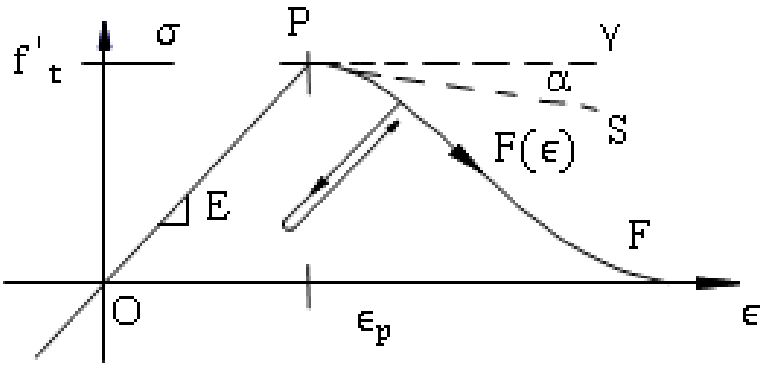

Fig. 1 Stress-strain diagram with strain-softening

Table 1 One-dimensional damage model

- Constitutive relation

$$\sigma = \overline{D}^{-1}\varepsilon \tag{1}$$

- Evolution equation

$$\dot{\overline{D}} = \frac{\dot{\bar{\gamma}} sign(\sigma)}{\sigma} \tag{2}$$

- Evolution equation for the hardening parameter $\bar{\xi}$

$$\dot{\bar{\xi}} = \dot{\bar{\gamma}} \tag{3}$$

- Yield function

$$\overline{\Phi}\left(\sigma, \bar{\xi}\right) = |\sigma| - (\sigma_f + K\bar{\xi}) \leq 0 \tag{4}$$

- Kuhn-Tucker complementary conditions (loading-unloading conditions)

$$\dot{\bar{\gamma}} > 0 \qquad \overline{\Phi}\left(\sigma, \bar{\xi}\right) \leq 0 \qquad \dot{\bar{\gamma}}\overline{\Phi}\left(\sigma, \bar{\xi}\right) = 0 \tag{5}$$

- Consistency condition

$$\dot{\bar{\gamma}}\dot{\overline{\Phi}}\left(\sigma, \bar{\xi}\right) = 0 \tag{6}$$

where $\overline{\mathrm{D}}$ is the compliance, $\bar{\gamma}$ is the "plastic/damage" multiplier, $\bar{\xi}$ is the hardening parameter, σ_f is the elastic limit, and K is the hardening coefficient.

2.1.2 Stress-strain rate form

We give here the detailed expressions of the evolution and constitutive equations (for the 1D case).

The complementary condition $\dot{\bar{\gamma}}\overline{\Phi} < 0$ implies that when $\overline{\Phi} < 0$ we will have $\dot{\bar{\gamma}} = 0$ and when $\dot{\bar{\gamma}} > 0$ we will have $\overline{\Phi} = 0$.

In the first case $\dot{\bar{\gamma}} = 0$ that is for elastic loading or unloading case, we have

$$\dot{\sigma} = \overline{D}^{-1}\dot{\varepsilon} + \dot{\overline{D}}^{-1}\varepsilon \tag{7}$$

Besides

$$\overline{D}\overline{D}^{-1} = 1 \quad \Leftrightarrow \dot{\overline{D}}\overline{D}^{-1} + \overline{D}\dot{\overline{D}}^{-1} = 0$$

$$\Longrightarrow \dot{\overline{D}}^{-1} = -\frac{\dot{\overline{D}}\overline{D}^{-1}}{\overline{D}} = -\overline{D}^{-1}\dot{\overline{D}}\overline{D}^{-1} \tag{8}$$

$$\dot{\sigma} = \overline{D}^{-1}\dot{\varepsilon} - \overline{D}^{-1}\dot{\overline{D}}\overline{D}^{-1}\varepsilon \tag{9}$$

$$\dot{\overline{D}} = \frac{\dot{\bar{\gamma}} sign(\sigma)}{\sigma} = 0$$

$$\dot{\sigma} = \overline{D}^{-1}\dot{\varepsilon} \tag{10}$$

In the second case $\dot{\gamma} > 0$ and consequently $\bar{\Phi} = 0$. Because $\bar{\Phi} = 0$ remains constant as long as $\dot{\gamma} > 0$ also the rate of $\bar{\Phi}$ vanishes, $\dot{\bar{\Phi}} = 0$, and we obtain

$$\begin{aligned}\dot{\bar{\Phi}} &= \frac{\partial \bar{\Phi}}{\partial \sigma}\dot{\sigma} + \frac{\partial \bar{\Phi}}{\partial \bar{\xi}}\dot{\bar{\xi}} \\ &= sign(\sigma)(\bar{D}^{-1}\dot{\varepsilon} + \dot{\bar{D}}^{-1}\varepsilon) - K\dot{\bar{\xi}} \\ &= sign(\sigma)\bar{D}^{-1}\dot{\varepsilon} + sign(\sigma)\dot{\bar{D}}^{-1}\varepsilon - K\dot{\bar{\gamma}} \\ &= sign(\sigma)\bar{D}^{-1}\dot{\varepsilon} - sign(\sigma)\bar{D}^{-1}\,\dot{\bar{D}}\bar{D}^{-1}\varepsilon - K\dot{\bar{\gamma}} \\ &= sign(\sigma)\bar{D}^{-1}\dot{\varepsilon} - sign(\sigma)\bar{D}^{-1}\frac{\dot{\bar{\gamma}}sign(\sigma)}{\sigma}\bar{D}^{-1}\varepsilon - K\dot{\bar{\gamma}} \\ &= sign(\sigma)\bar{D}^{-1}\dot{\varepsilon} - \dot{\bar{\gamma}}(\bar{D}^{-1} + K) = 0\end{aligned} \tag{11}$$

$$\Longrightarrow \dot{\bar{\gamma}} = \frac{\bar{D}^{-1}}{\bar{D}^{-1}+K}\dot{\varepsilon}sign(\sigma) \tag{12}$$

$$\dot{\bar{D}} = \frac{\dot{\bar{\gamma}}sign(\sigma)}{\sigma} = \frac{\bar{D}^{-1}\dot{\varepsilon}}{(\bar{D}^{-1}+K)\sigma} \tag{13}$$

$$\begin{aligned}\dot{\sigma} &= \bar{D}^{-1}\dot{\varepsilon} - \bar{D}^{-1}\dot{\bar{D}}\bar{D}^{-1}\varepsilon \\ &= \bar{D}^{-1}\dot{\varepsilon} - \bar{D}^{-1}\frac{\bar{D}^{-1}\dot{\varepsilon}}{(\bar{D}^{-1}+K)\sigma}\bar{D}^{-1}\varepsilon \\ &= \bar{D}^{-1}\dot{\varepsilon} - \bar{D}^{-1}\frac{\bar{D}^{-1}\dot{\varepsilon}}{\bar{D}^{-1}+K} \\ &= \bar{D}^{-1}\dot{\varepsilon}\left(1 - \frac{\bar{D}^{-1}}{\bar{D}^{-1}+K}\right) \\ &= \frac{\bar{D}^{-1}K}{\bar{D}^{-1}+K}\dot{\varepsilon}\end{aligned} \tag{14}$$

Hence, we obtain the following form for stress rate equation

$$\dot{\sigma} = \begin{cases}\bar{D}^{-1}\dot{\varepsilon}\,;\ \dot{\bar{\gamma}} = 0 \\ \frac{\bar{D}^{-1}K}{\bar{D}^{-1}+K}\dot{\varepsilon}\,;\ \dot{\bar{\gamma}} > 0\end{cases} \quad \text{or} \quad \frac{\partial\sigma}{\partial\varepsilon} = \begin{cases}\bar{D}^{-1}\,;\ \dot{\bar{\gamma}} = 0 \\ \frac{\bar{D}^{-1}K}{\bar{D}^{-1}+K};\ \dot{\bar{\gamma}} > 0\end{cases} \tag{15}$$

The stress response of a body subjected to the strain evolution with pseudo time *t* shown in Fig. 2 is given in Fig. 3.

2.1.3 Return mapping

In the previous section, the theoretical 1D formulation of the elastodamage model was presented. We present here the key points of the numerical integration of such a model.

Let's consider a time step t_{n+1} with a given corresponding strain ε_{n+1} and previously converged internal variables $\bar{\xi}_n$ and $\bar{D}_n$. The numerical integration is here performed considering a return mapping algorithm where we first consider no evolution of internal variables at time step t_{n+1} which leads to the definition of a trial stat

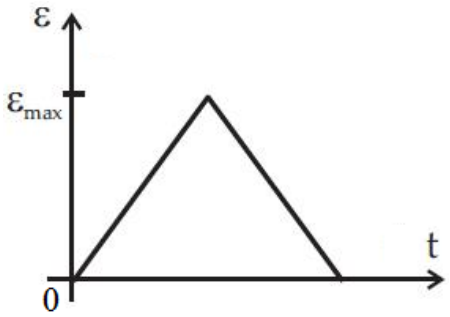

Fig. 2 Strain evolution with pseudo time *t*

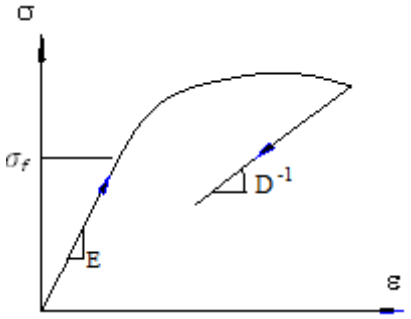

Fig. 3 Stress-strain diagram for 1D damage model in loading-unloading cycle

$$\bar{\xi}_{n+1}^{trial} = \bar{\xi}_n \;\; \bar{D}_{n+1}^{trial} = \bar{D}_n \;\text{ and }\; \sigma_{n+1}^{trial} = \bar{D}_n^{-1}\varepsilon_{n+1} \tag{16}$$

The Yield function is then checked: $\bar{\Phi}_{n+1}^{trial} = \bar{\Phi}(\sigma_{n+1}^{trial}, \bar{\xi}_{n+1}^{trial})$. If $\bar{\Phi}_{n+1}^{trial} < 0$ then the trial state is admissible. If $\bar{\Phi}_{n+1}^{trial} > 0$, internal variables and stress state have to be updated so that $\bar{\Phi}_{n+1} = \bar{\Phi}(\sigma_{n+1}, \bar{\xi}_{n+1}) = 0$.

The expression of σ_{n+1} can be given in terms of the trial stress state σ_{n+1}^{trial} as

$$\sigma_{n+1} = \bar{D}_{n+1}^{-1}\varepsilon_{n+1} = (\bar{D}_{n+1}^{-1} + \bar{D}_n^{-1} - \bar{D}_n^{-1})\varepsilon_{n+1}$$

$$= \bar{D}_n^{-1}\varepsilon_{n+1} + \left(\frac{1}{\bar{D}_{n+1}} - \frac{1}{\bar{D}_n}\right)\varepsilon_{n+1}$$

$$= \sigma_{n+1}^{trial} + \frac{\bar{D}_n - \bar{D}_{n+1}}{\bar{D}_n \bar{D}_{n+1}}\varepsilon_{n+1}$$

$$= \sigma_{n+1}^{trial} - \frac{\bar{\gamma}_{n+1} sign(\sigma_{n+1})}{\bar{D}_n \bar{D}_{n+1} \sigma_{n+1}} \varepsilon_{n+1}$$

$$= \sigma_{n+1}^{trial} - \bar{D}_n^{-1} \bar{\gamma}_{n+1} sign(\sigma_{n+1}) \tag{17}$$

Inserting this expression into the incremental equations leads to

$$\begin{aligned} \sigma_{n+1} &= \sigma_{n+1}^{trial} - \bar{D}_n^{-1} \bar{\gamma}_{n+1} sign(\sigma_{n+1}) \\ \bar{D}_{n+1} &= \bar{D}_n + \frac{\bar{\gamma}_{n+1} sign(\sigma_{n+1})}{\sigma_{n+1}} \\ \bar{\xi}_{n+1} &= \bar{\xi}_n + \bar{\gamma}_{n+1} \\ \bar{\Phi}_{n+1} &= |\sigma_{n+1}| - \left(\sigma_f + K \bar{\xi}_{n+1}\right) = 0 \end{aligned} \tag{18}$$

This is a set of 4 algebraic equations to be solved for the unknowns $\sigma_{n+1},\ D_{n+1},\ \xi_{n+1},\ \bar{\gamma}_{n+1}$

2.1.4 Analytical solution of (18)

The sign of the stress equals the sign of the trial stress

$$\sigma_{n+1} = |\sigma_{n+1}| sign(\sigma_{n+1}) = \left|\sigma_{n+1}^{trial}\right| sign(\sigma_{n+1}^{trial}) - \bar{D}_n^{-1} \bar{\gamma}_{n+1} sign(\sigma_{n+1})$$

$$\Leftrightarrow (|\sigma_{n+1}| + \bar{D}_n^{-1} \bar{\gamma}_{n+1}) sign(\sigma_{n+1}) = \left|\sigma_{n+1}^{trial}\right| sign(\sigma_{n+1}^{trial})$$

$$\Rightarrow \begin{cases} sign(\sigma_{n+1}) = sign(\sigma_{n+1}^{trial}) \\ |\sigma_{n+1}| + \bar{D}_n^{-1} \bar{\gamma}_{n+1} = \left|\sigma_{n+1}^{trial}\right| \end{cases} \tag{19}$$

With this result in hand, we find

$$\bar{\Phi}_{n+1} = |\sigma_{n+1}| - \left(\sigma_f + K \bar{\xi}_{n+1}\right) = 0$$

$$= \left|\sigma_{n+1}^{trial}\right| - \bar{D}_n^{-1} \bar{\gamma}_{n+1} - \left[\sigma_f + K\left(\bar{\xi}_{n+1} - \bar{\xi}_n + \bar{\xi}_n\right)\right]$$

$$= \left|\sigma_{n+1}^{trial}\right| - \left(\sigma_f + K \bar{\xi}_n\right) - K\left(\bar{\xi}_{n+1} - \bar{\xi}_n\right) - \bar{D}_n^{-1} \bar{\gamma}_{n+1}$$

$$= \bar{\Phi}_{n+1}^{trial} - K \bar{\gamma}_{n+1} - \bar{D}_n^{-1} \bar{\gamma}_{n+1}$$

$$= \bar{\Phi}_{n+1}^{trial} - \bar{\gamma}_{n+1} (\bar{D}_n^{-1} + K) = 0$$

and finally

$$\bar{\gamma}_{n+1} = \frac{\bar{\Phi}_{n+1}^{trial}}{\bar{D}_n^{-1} + K} \tag{20}$$

which allows with (18) to update all internal variables and stress state.

2.2 Softening part

2.2.1 Model summary

Table 2 Model summary for softening part

- Constitutive relation

$$t = \bar{D}^{-1}(\mathbf{Bd} + \bar{G}\alpha)$$

- Evolution equations for internal variables

$$\dot{\bar{D}} = \frac{\dot{\bar{\gamma}} sign(t)}{t} \tag{21}$$

$$\dot{\bar{\xi}} = \dot{\bar{\gamma}} \tag{22}$$

$$\dot{\alpha} = \dot{\bar{\gamma}} sign(t) \tag{23}$$

- Yield function

$$\bar{\Phi}\left(t, \bar{\xi}\right) = |t| - (\sigma_u + K_s \bar{\xi}) \leq 0 \tag{24}$$

- Kuhn-Tucker complementary conditions (loading-unloading conditions)

$$\dot{\bar{\gamma}} > 0 \qquad \bar{\Phi}\left(t, \bar{\xi}\right) \leq 0 \qquad \dot{\bar{\gamma}} \bar{\Phi}\left(t, \bar{\xi}\right) = 0 \tag{25}$$

- Consistency condition

$$\dot{\bar{\gamma}} \dot{\bar{\Phi}}\left(t, \bar{\xi}\right) = 0 \tag{26}$$

where t is the traction force acting at discontinuity, α is the crack opening (incompatible mode parameter), $\bar{D}$ is the discontinuity compliance, $\bar{\gamma}$ is the softening damage multiplier, $\bar{\xi}$ is the softening parameter (displacement-like variable), σ_u is the ultimate stress, and K_s is the softening coefficient.

2.2.2 Rate form

The complementary condition $\dot{\bar{\gamma}} \bar{\Phi} < 0$ implies that when $\bar{\Phi} < 0$ we will have $\dot{\bar{\gamma}} = 0$ and when $\dot{\bar{\gamma}} > 0$ we will have $\bar{\Phi} = 0$.

In the first case $\dot{\bar{\gamma}} = 0$, we have

$$\begin{aligned} \dot{t} &= \bar{\bar{D}}^{-1}\dot{\alpha} + \dot{\bar{\bar{D}}}^{-1}\alpha \\ &= \bar{\bar{D}}^{-1}\dot{\alpha} - \bar{\bar{D}}^{-1}\dot{\bar{D}}\bar{\bar{D}}^{-1}\alpha \end{aligned} \tag{27}$$

$$\dot{\bar{D}} = \frac{\dot{\bar{\gamma}} sign(t)}{t} = 0 \tag{28}$$

$$\Rightarrow \dot{t} = \bar{\bar{D}}^{-1}\dot{\alpha} \tag{29}$$

In the second case $\dot{\bar{\gamma}} > 0$ and consequently $\bar{\Phi} = 0$

$$\bar{\Phi} = |t| - (\sigma_u - \bar{q}) = 0 \tag{30}$$

$$\Rightarrow t = (\sigma_u - \bar{q}) sign(t)$$

$$\Rightarrow \dot{t} = -\dot{\bar{q}} sign(t) = -\frac{\partial \bar{q}}{\partial \bar{\xi}} \frac{\partial \bar{\xi}}{\partial t} sign(t) = -\frac{\partial \bar{q}}{\partial \bar{\xi}} \dot{\bar{\xi}} sign(t) = -\frac{\partial \bar{q}}{\partial \bar{\xi}} \dot{\bar{\gamma}} sign(t) = -\frac{\partial \bar{q}}{\partial \bar{\xi}} \dot{\alpha}$$

$$\Rightarrow \frac{\dot{t}}{\dot{\alpha}} = -\frac{\partial \bar{\bar{q}}}{\partial \bar{\bar{\xi}}} \tag{31}$$

Besides

$$\bar{\bar{q}} = \sigma_u \left(1 - e^{-\beta \bar{\bar{\xi}}}\right) \tag{32}$$

$$\Rightarrow \frac{\dot{t}}{\dot{\alpha}} = -\frac{\partial \bar{\bar{q}}}{\partial \bar{\bar{\xi}}} = -\sigma_u \beta e^{-\beta \bar{\bar{\xi}}} \Leftrightarrow \dot{t} = -\sigma_u \beta e^{-\beta \bar{\bar{\xi}}} \dot{\alpha} \tag{33}$$

Hence, we obtain the following form for stress rate equation:

$$\dot{t} = \begin{cases} \bar{\bar{D}}^{-1} \dot{\alpha} \; ; \; \dot{\bar{\bar{\gamma}}} = 0 \\ -\sigma_u \beta e^{-\beta \bar{\bar{\xi}}} \dot{\alpha} \; ; \; \dot{\bar{\bar{\gamma}}} > 0 \end{cases} \quad \text{or} \quad \frac{\partial t}{\partial \alpha} = \begin{cases} \bar{\bar{D}}^{-1}; \; \dot{\bar{\bar{\gamma}}} = 0 \\ -\sigma_u \beta e^{-\beta \bar{\bar{\xi}}}; \; \dot{\bar{\bar{\gamma}}} > 0 \end{cases} \tag{34}$$

2.2.3 Find $t_{n+1}^{trial}, \bar{\bar{\gamma}}_{n+1}^{trial}$

We further discuss the solution method in the context of the backward-Euler implicit time integration scheme (e.g., see Ibrahimbegovic (2009)), which is used to integrate these rate constitutive equations. By first assuming that the state remains elastic, we will obtain so-called elastic trial state where crack opening will not change in the particular time step. We have

$$\begin{cases} t_{n+1}^{trial} = \sigma_{n+1}^{trial} \\ t_{n+1}^{trial} = \bar{\bar{D}}_{n+1}^{trial,-1} \alpha_{n+1}^{trial} \end{cases} \Rightarrow \alpha_{n+1}^{trial} = \bar{\bar{D}}_{n+1}^{trial} t_{n+1}^{trial} = \bar{\bar{D}}_n t_{n+1}^{trial} = \bar{\bar{D}}_n \sigma_{n+1}^{trial} \tag{35}$$

$$\begin{aligned} \sigma_{n+1}^{trial} &= \bar{D}_n^{-1} \left(\mathbf{Bd_{n+1}} + \bar{G} \alpha_{n+1}^{trial} \right) \\ &= \bar{D}_n^{-1} \left(\mathbf{Bd_{n+1}} + \bar{G} \bar{\bar{D}}_n \sigma_{n+1}^{trial} \right) \end{aligned} \tag{36}$$

$$\Rightarrow \left(\bar{D}_n - \bar{G} \bar{\bar{D}}_n \right) \sigma_{n+1}^{trial} = \mathbf{Bd_{n+1}}$$

$$\Rightarrow t_{n+1}^{trial} = \sigma_{n+1}^{trial} = \frac{\mathbf{Bd_{n+1}}}{\bar{D}_n - \bar{G} \bar{\bar{D}}_n} = \frac{\varepsilon_{n+1}}{\bar{D}_n + \frac{1}{l^e} \bar{\bar{D}}_n} \tag{37}$$

$$\bar{\bar{\Phi}}_{n+1} = |t_{n+1}| - \left(\sigma_u + K_s \bar{\bar{\xi}}_{n+1} \right) = t_{n+1} sign(t_{n+1}) - \left(\sigma_u + K_s \bar{\bar{\xi}}_{n+1} \right) \tag{38}$$

where

$$\begin{aligned} t_{n+1} &= \sigma_{n+1} = \bar{D}_n^{-1} (\mathbf{Bd_{n+1}} + \bar{G} \alpha_{n+1}) \\ \alpha_{n+1} &= (\alpha_n^{max} + \bar{\bar{\gamma}}_{n+1}) sign(t_{n+1}) \\ \alpha_n^{max} &= \bar{\bar{D}}_n t_n^{max} \\ t_n^{max} &= \sigma_u + K_s \bar{\bar{\xi}}_n \end{aligned} \tag{39}$$

Thus

$$\alpha_n^{max} = \bar{\bar{D}}_n \left(\sigma_u + K_s \bar{\bar{\xi}}_n \right) \tag{40}$$

$$\alpha_{n+1} = \left[\bar{\bar{D}}_n \left(\sigma_u + K_s \bar{\bar{\xi}}_n \right) + \bar{\bar{\gamma}}_{n+1} \right] sign(t_{n+1}) \tag{41}$$

$$t_{n+1} = \sigma_{n+1} = \bar{D}_n^{-1} \left\{ \mathbf{Bd_{n+1}} + \bar{G} \left[\bar{\bar{D}}_n \left(\sigma_u + K_s \bar{\bar{\xi}}_n \right) + \bar{\bar{\gamma}}_{n+1} \right] sign(t_{n+1}) \right\} \tag{42}$$

$$\bar{\bar{\Phi}}_{n+1} = \bar{D}_n^{-1} \left\{ \mathbf{Bd_{n+1}} sign(t_{n+1}) + \bar{G} \left[\bar{\bar{D}}_n \left(\sigma_u + K_s \bar{\bar{\xi}}_n \right) + \bar{\bar{\gamma}}_{n+1} \right] \right\} - \left[\sigma_u + K_s \left(\bar{\bar{\xi}}_n + \bar{\bar{\gamma}}_{n+1} \right) \right] \tag{43}$$

$$\bar{\bar{\Phi}}_{n+1} = 0$$

$$\Leftrightarrow\ \bar{D}_n^{-1}\left[\mathbf{Bd_{n+1}}sign(t_{n+1}) + \bar{G}\bar{\bar{D}}_n\left(\sigma_u + K_s\bar{\bar{\xi}}_n\right) + \bar{G}\bar{\bar{\gamma}}_{n+1}\right] - \left(\sigma_u + K_s\bar{\bar{\xi}}_n\right) - K_s\bar{\bar{\gamma}}_{n+1} = 0$$

$$\Leftrightarrow\ \mathbf{Bd_{n+1}}sign(t_{n+1}) + \bar{G}\bar{\bar{D}}_n\left(\sigma_u + K_s\bar{\bar{\xi}}_n\right) + \bar{G}\bar{\bar{\gamma}}_{n+1} - \bar{D}_n\left(\sigma_u + K_s\bar{\bar{\xi}}_n\right) - K_s\bar{D}_n\bar{\bar{\gamma}}_{n+1} = 0$$

$$\Leftrightarrow\ \mathbf{Bd_{n+1}}sign(t_{n+1}) + \left(\bar{G}\bar{\bar{D}}_n - \bar{D}_n\right)\left(\sigma_u + K_s\bar{\bar{\xi}}_n\right) = (K_s\bar{D}_n - \bar{G})\bar{\bar{\gamma}}_{n+1}$$

$$\left|t_{n+1}^{trial}\right|$$

$$\Leftrightarrow\ \underbrace{\frac{\overbrace{\mathbf{Bd_{n+1}}sign(t_{n+1})}}{\bar{D}_n - \bar{G}\bar{\bar{D}}_n} - \left(\sigma_u + K_s\bar{\bar{\xi}}_n\right)}_{\bar{\bar{\Phi}}_{n+1}^{trial}} = \frac{K_s\bar{D}_n - \bar{G}}{\bar{D}_n - \bar{G}\bar{\bar{D}}_n}\bar{\bar{\gamma}}_{n+1}$$

$$\Rightarrow\ \bar{\bar{\gamma}}_{n+1} = \frac{\bar{\bar{\Phi}}_{n+1}^{trial}\left(\bar{D}_n - \bar{G}\bar{\bar{D}}_n\right)}{K_s\bar{D}_n - \bar{G}} = \frac{\bar{\bar{\Phi}}_{n+1}^{trial}\left(\bar{D}_n + \frac{1}{l^e}\bar{\bar{D}}_n\right)}{K_s\bar{D}_n + \frac{1}{l^e}} \tag{44}$$

3. Reference solution in a bar – Analytical solution of dynamic strain-softening

Consider a bar of length *2L*, with a unit cross-sectional area and a mass density ρ per unit length. Let the bar be loaded by forcing both ends to move simultaneously outward, with constant opposite velocities of magnitude *v*. The longitudinal coordinate *x* is measured from the bar's center (Fig. 4). The boundary conditions are

$$\begin{cases} \text{For } x = -L\text{: } u = -vt \\ \text{For } x = L\text{: } u = vt \end{cases} \quad (\text{for } t \geq 0) \tag{45}$$

Two step waves are generated in the bar. One wave travels from the right boundary in the negative *x*-direction. The other wave travels from the left boundary in the positive *x*-direction. The two step waves of constant strain travel to the center of the bar and meet at $x = 0$ for the time $t = L/c_e$. When the two waves meet strain doubles instantaneously at the center of the bar if $\varepsilon \leq \varepsilon_p/2$ and the midsection enters immediately the strain-softening regime with an increase to infinite strain if $\varepsilon_p/2 < \varepsilon \leq \varepsilon_p$, with the latter representing the strain value which triggers softening.

Before the onset of strain-softening the problem is governed by the differential equation of motion with the elastic wave speed $c_e = \sqrt{\frac{E}{\rho}}$. This standard equation is the wave equation, which is hyperbolic for real wave speeds.

$$c_e^2\frac{\partial^2 u}{\partial x^2} = \frac{\partial^2 u}{\partial t^2} \tag{46}$$

The longitudinal displacement function in the linear elastic domain is derived from appropriate initial and boundary conditions.

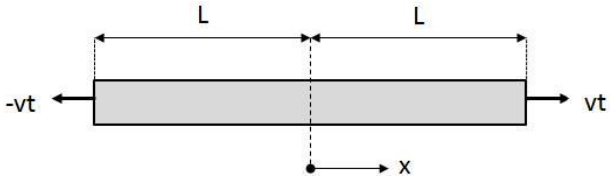

Fig. 4 Geometry and loading of strain-softening bar

$$u(x,t) = -v\,\langle t - \frac{x+L}{c_e}\rangle + v\,\langle t + \frac{x-L}{c_e}\rangle \tag{47}$$

in which the symbol $\langle\ \rangle$ is defined as $\langle\, A\,\rangle = A$ if $A > 0$ and $\langle\, A\,\rangle = 0$ if $A \leq 0$

The corresponding strain function needs to be positive. Accordingly, the Heaviside step function H is used.

$$\varepsilon = \frac{\partial u}{\partial x} = \frac{v}{c_e}\left[H\left(t - \frac{x+L}{c_e}\right) + H\left(t + \frac{x-L}{c_e}\right)\right] \tag{48}$$

The stress caused by the deformation is described with Hooke's law for linear elasticity.

$$\sigma = E\varepsilon \tag{49}$$

Obviously, if $\varepsilon \leq \varepsilon_p/2$, the assumption of elastic behavior holds for $t \leq 2L/c_e$, i.e., until the time each wave-front runs the entire length of the bar. If, however, $\varepsilon_p/2 < \varepsilon \leq \varepsilon_p$, the solution for the displacement *u(x,t)* in Eq. (47) holds only for $t \leq L/c_e$.

The slope of the stress-strain diagram in the strain-softening domain is $F'(\varepsilon)$ that is less than zero. Because $F'(\varepsilon) < 0$, the differential equation of motion in the strain-softening domain is elliptic, which means that interaction over finite distances is immediate.

$$c_e^2\frac{\partial^2 u}{\partial x^2} + \frac{\partial^2 u}{\partial t^2} = 0 \qquad \text{with } c_e^2 = \frac{F'(\varepsilon)}{\rho} \tag{50}$$

Strain-softening is limited to an area around $x = 0$. The displacements develop a discontinuity at $x = 0$, with a jump of magnitude $4v\langle t - L/c_e\rangle$. Strain starts to increase infinitely and stress drops to zero in the strain-softening zone. The rest of the bar starts to unload elastically.

Strain near $x = 0$, i.e., at the center of the bar can be expressed by the Dirac Delta function

$$\varepsilon = 4v\langle t - L/c_e\rangle\delta(x) \tag{51}$$

The solution for the strain field outside the strain – softening zone, $t > L/c_e$ and $x < 0$, is

$$\varepsilon = \frac{v}{c_e}\left[H\left(t - \frac{x+L}{c_e}\right) + H\left(t + \frac{x-L}{c_e}\right) + 4v\langle t - L/c_e\rangle\delta(x)\right] \tag{52}$$

For the right half of the bar, $x > 0$, a symmetric solution applies.

4. Numerical implementation: Finite element with embedded strong discontinuities

4.1 Standard finite element interpolation

The displacement interpolation for one-dimensional truss bar with 2 nodes can be written as

$$u(x) = \sum_{a=1}^{2} N_a(x) u_a = \mathbf{Nu} \tag{53}$$

where **u** represents nodal displacement vector.

For this case of element, we use standard linear interpolation functions for continuum displacement approximation

$$\mathbf{N} = \left\{ N_1(x) = 1 - \frac{x}{l^e}, N_2(x) = \frac{x}{l^e} \right\} \tag{54}$$

The strain interpolation can be obtained from the displacement field resulting in

$$\varepsilon(x) = \frac{du(x)}{dx} = \mathbf{Bu} \tag{55}$$

where **B** is the strain-displacement matrix

$$\mathbf{B} = \frac{d\mathbf{N}}{dx} = \frac{1}{l^e}[-1 \;\; 1] \tag{56}$$

4.2 Strong discontinuity kinematics

Once the localized failure occurs, the crack opening (further denoted as α, see Fig. 6) contributes to a "jump" or irregular part in the displacement field. Thus, the total displacement field is the sum of regular (smooth) part and irregular part.

$$u(x,t) = \hat{u}(x,t) + \alpha\left\{H_{x_c}(x) - \varphi(x)\right\} \tag{57}$$

$$u(x,t) = \hat{u}(x,t) - \alpha\varphi(x) + \alpha H_{x_c}(x) \tag{58}$$

where $H_{x_c}(x)$ is the Heaviside function introducing the displacement jump.

$$H_{x_c}(x) = \begin{cases} 1; x > x_c \\ 0; x < x_c \end{cases} \tag{59}$$

and $\varphi(x)$ is a (smooth) function, introduced to limit the influence of the displacement jump within the "failure" domain. Usual choice for $\varphi(x)$ in the finite element implementation pertains to the shape function of selected interpolation. For a 1D truss-bar with 2 nodes, we can choose

$$\varphi(x) = N_2(x) = \frac{x}{l^e} \tag{60}$$

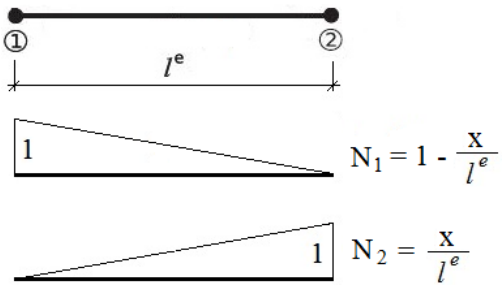

Fig. 5 Shape functions

The corresponding illustrations for $H_{x_c}(x)$ and $\varphi(x)$ for a two-node truss-bar element are given in Fig. 7.

Denoting with $\bar{u}(x,t) = \hat{u}(x,t) - \alpha\varphi(x)$ the continuous part of the displacement field, and with α the "jump" in displacement, we can further write additive decomposition of displacement field

$$u(x,t) = \bar{u}(x,t) + \alpha H_{x_c}(x) \tag{61}$$

$$u(x,t) = \bar{u}(x,t) + \alpha\varphi(x) + \alpha\underbrace{\{H_{x_c}(x) - \varphi(x)\}}_{M(x)} \tag{62}$$

$$u(x,t) = \bar{u}(x,t) + \alpha N_2(x) + \alpha\{H_{x_c}(x) - N_2(x)\} \tag{63}$$

In Eq. (62) above, $M(x)$ is the additional interpolation function (see Fig. 7), and can be used alongside standard interpolation function to describe the heterogeneous displacement field with activated jump inside the finite element. The $M(x)$ is defined as follows

$$M(x) = \begin{cases} -\frac{x}{l^e}; x \in [0, x_c\rangle \\ 1 - \frac{x}{l^e}; x \in \langle x_c, l^e] \end{cases} \tag{64}$$

The finite element displacement interpolation can thus be stated as

$$u(x) = \sum_{a=1}^{2} N_a(x)u_a + \alpha M(x) \tag{65}$$

The corresponding strain field can then be obtained by exploiting the kinematic relation

$$\varepsilon(x,t) = \sum_{a=1}^{2} B_a(x)u_a + \alpha G(x) \tag{66}$$

where

$$G(x) = G + \delta_{x_c} = -\frac{1}{l^e} + \delta_{x_c}, x \in [0, l^e] \tag{67}$$

and $\delta_{x_c} = \begin{cases} \infty; x = x_c \\ 0; \text{otherwise} \end{cases}$ – Dirac's Delta function

4.3 Computational procedure

The solution will be computed at discrete time values 0, t_1, t_2,…, t by means of incremental iterative scheme. The local phase will be treated separately from global phase

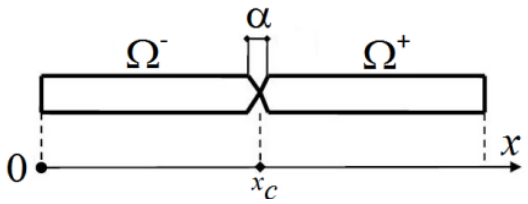

Fig. 6 Displacement discontinuity at localized failure for the mechanical load

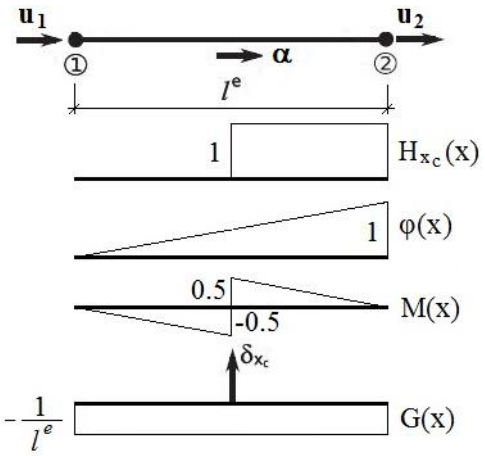

Fig. 7 Displacement discontinuity for 2-node bar element: Heaviside function, smooth function and additional interpolation function

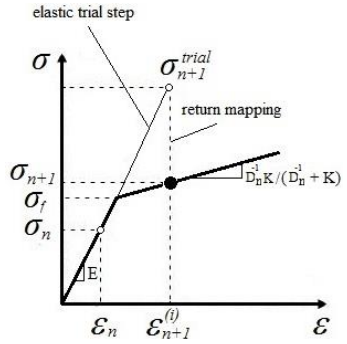

Fig. 8 Return mapping algorithm

The local (element) computation should provide the values of internal variables at the end of time step guaranteeing the plastic admissibility of the stress field. Implicit backward Euler scheme will be taken for time integration of evolution equations.

Given: $d_{n+1}, \overline{D}_n, \bar{\xi}_n, \alpha_n, \overline{\overline{D}}_n, \bar{\bar{\xi}}_n, \Delta t = t_{n+1} - t_n$

Find: $\bar{\xi}_{n+1}, \overline{D}_{n+1}, \alpha_{n+1}, \bar{\bar{\xi}}_{n+1}, \overline{\overline{D}}_{n+1}$

In the global phase, we compute the current iterative values of nodal displacements at t_{n+1} while keeping other variables fixed.

Given: d_{n+1}, α_{n+1}

Find: $d_{n+1} = d_n + \Delta d_{n+1}$

The subscript *n* denotes the values of variables at the discrete time value t_n. First, we need to solve the elastodamage part of the task, and once reached the ultimate stress, deal with localized failure and the softening phase.

The local computation for the elastodamage phase can be summarized in the following Return Mapping Algorithm:

Initial data: $\bar{\bar{D}}_n, \bar{\xi}_n$

Strain: $\varepsilon_{n+1} = \sum_{a=1}^{2} \boldsymbol{B}_a d_{a,n+1}$ (69)

Compute elastic trial stress and test for damage loading

$$\sigma_{n+1}^{\text{trial}} = \bar{D}_n^{-1} \varepsilon_{n+1} \tag{70}$$

$$\bar{\Phi}_{n+1}^{\text{trial}} = \left|\sigma_{n+1}^{\text{trial}}\right| - \left(\sigma_f + \underbrace{K\bar{\xi}_n}_{-\bar{q}_n}\right) \tag{71}$$

If $\bar{\Phi}_{n+1}^{\text{trial}} \leq 0$ **then**

Elastic step: $\sigma_{n+1} = \sigma_{n+1}^{\text{trial}}; C_{n+1}^{ed} = \bar{D}_n^{-1}$ (72)

Exit

Else

$$\bar{\gamma}_{n+1} = \frac{\bar{\Phi}_{n+1}^{\text{trial}}}{\bar{D}_n^{-1} + K} \tag{73}$$

$$\sigma_{n+1} = \sigma_{n+1}^{\text{trial}} - \bar{D}_n^{-1} \bar{\gamma}_{n+1} sign(\sigma_{n+1}^{\text{trial}}) \tag{74}$$

$$\bar{\xi}_{n+1} = \bar{\xi}_n + \bar{\gamma}_{n+1} \tag{75}$$

$$\bar{D}_{n+1} = \bar{D}_n + \frac{\bar{\gamma}_{n+1} sign(\sigma_{n+1}^{\text{trial}})}{\sigma_{n+1}} \tag{76}$$

$$C_{n+1}^{ed} = \frac{\bar{D}_{n+1}^{-1} K}{\bar{D}_{n+1}^{-1} + K} \tag{77}$$

End

Once the ultimate stress σ_u is reached, we carry on with solving the softening part of the task. Similar to hardening part, the local computation for this phase is summarized in the Return Mapping Algorithm as follows

Initial data: $\bar{D}_n, \bar{\bar{D}}_n, \bar{\bar{\xi}}_n$

Compute elastic trial traction force and test for damage loading

$$t_{n+1}^{trial} = \frac{\varepsilon_{n+1}}{\bar{D}_n + \frac{1}{l^e}\bar{\bar{D}}_n} \tag{78}$$

$$\bar{\bar{\Phi}}_{n+1}^{\text{trial}} = \left|t_{n+1}^{\text{trial}}\right| - \left(\sigma_u + \underbrace{K_s \bar{\bar{\xi}}_n}_{-\bar{\bar{q}}_n}\right) \tag{79}$$

If $\bar{\bar{\Phi}}_{n+1}^{\text{trial}} \leq 0$ **then**

Elastic step: $t_{n+1} = t_{n+1}^{\text{trial}}$ (80)

Exit

Else

$$\bar{\bar{\gamma}}_{n+1} = \frac{\bar{\bar{\Phi}}_{n+1}^{trial}\left(\bar{D}_n + \frac{1}{l^e}\bar{\bar{D}}_n\right)}{K_s \bar{D}_n + \frac{1}{l^e}} \tag{81}$$

$$\alpha_{n+1} = \alpha_n + \bar{\bar{\gamma}}_{n+1} sign\left(t_{n+1}^{\text{trial}}\right) \tag{82}$$

$$\bar{\bar{\xi}}_{n+1} = \bar{\bar{\xi}}_n + \bar{\bar{\gamma}}_{n+1} \tag{83}$$

$$\bar{\bar{q}}_{n+1} = \sigma_u\left(1 - e^{-\beta \bar{\bar{\xi}}_{n+1}}\right) \tag{84}$$

$$t_{n+1} = (\sigma_u - \bar{\bar{q}}_{n+1}) sign\left(t_{n+1}^{\text{trial}}\right) \tag{85}$$

$$\bar{\bar{D}}_{n+1} = \bar{\bar{D}}_n + \frac{\bar{\bar{\gamma}}_{n+1} sign(t_{n+1})}{t_{n+1}} \tag{86}$$

End

After the local computation is finished and the values of internal variables obtained, we turn to the global phase in order to provide new iterative values of nodal displacements. In this phase, we consider the numerical simulations by implicit Newmark scheme and Newton-Raphson method.

The system of linearized equations can be written as

$$\begin{bmatrix} \mathbb{A}_{e=1}^{n_{el}} \widehat{\mathbf{K}}^{(e)} & \mathbb{A}_{e=1}^{n_{el}} \mathbf{F}^{(e)} \\ \mathbf{F}^{(e),T} & \mathbf{H}^{(e)} \end{bmatrix}_{n+1}^{i} \begin{pmatrix} \Delta \mathbf{d}_{n+1}^{(e),(i)} \\ \Delta \boldsymbol{\alpha}_{n+1}^{(e),(i)} \end{pmatrix} = \begin{pmatrix} \mathbb{A}_{e=1}^{n_{el}} \mathbf{r}_{n+1}^{(e),(i)} \\ \mathbf{h}_{n+1}^{(e),(i)} \end{pmatrix} \tag{87}$$

in which the parts of element stiffness matrix are as follows

$$\widehat{\mathbf{K}}_{n+1}^{(e),(i)} = \mathbf{K}_{n+1}^{(e),(i)} + \frac{1}{\beta(\Delta t)^2} \mathbf{M}_{n+1}^{(e),(i)} \tag{88}$$

$$\mathbf{K}_{n+1}^{(e),(i)} = \int_0^{l^e} \mathbf{B}^T C_{n+1} \mathbf{B} dx \tag{89}$$

$$\mathbf{F}_{n+1}^{(e),(i)} = \int_0^{l^e} \mathbf{B}^T C_{n+1} \bar{\mathbf{G}} dx \tag{90}$$

$$\mathbf{H}_{n+1}^{(e),(i)} = \int_0^{l^e} \bar{\mathbf{G}}^T C_{n+1} \bar{\mathbf{G}} dx + \frac{\partial t_{n+1}}{\partial \alpha_{n+1}} \tag{91}$$

and $\mathbf{r}^{(e)}$ and $\mathbf{h}^{(e)}$ are residuals

$$\mathbf{r}_{n+1}^{(e),(i)} = \mathbf{f}_{ext,n+1}^{(e),(i)} - \mathbf{f}_{int,n+1}^{(e),(i)} - \mathbf{M}_{n+1}^{(e),(i)} \mathbf{a}_{n+1}^{(e),(i)} \tag{92}$$

$$\mathbf{h}_{n+1}^{(e),(i)} = \int_0^{l^e} \bar{\mathbf{G}}^T \sigma_{n+1}^{(e),(i)} dx + t_{n+1}^{(e),(i)} \tag{93}$$

with *t* is the traction force acting at discontinuity.

In Eq. (88) above, $\mathbf{M}^{(e)}$ is the element mass matrix.

$$\mathbf{M}_{\mathbf{n+1}}^{(\mathbf{e}),(\mathbf{i})} = \int_{\Omega} \rho \mathbf{N}^T \mathbf{N} d\Omega \tag{94}$$

and $\mathbf{f}_{ext}^{(e)}$ and $\mathbf{f}_{int}^{(e)}$ in Eq. (92) are external and internal forces, respectively.

$$\mathbf{f}_{ext,n+1}^{(e),(i)} = \int_{\Omega} \mathbf{N} \mathbf{b} \mathbf{N}^{\boldsymbol{T}} d\Omega + [\mathbf{N}^{\boldsymbol{T}} \bar{t}]_{\Gamma_{\sigma}} \tag{95}$$

$$\mathbf{f}_{int,n+1}^{(e),(i)} = \int_{\boldsymbol{\Omega}} \mathbf{B}^T \sigma d\Omega \tag{96}$$

4.4 Static condensation

One of the main features of finite element framework with embedded strong discontinuities is the ability to statically condense out the local element parameters on the element level, leaving the focus again on the solution of the global problem in terms of the global displacement field **d**. Then, the final statically condensed system is

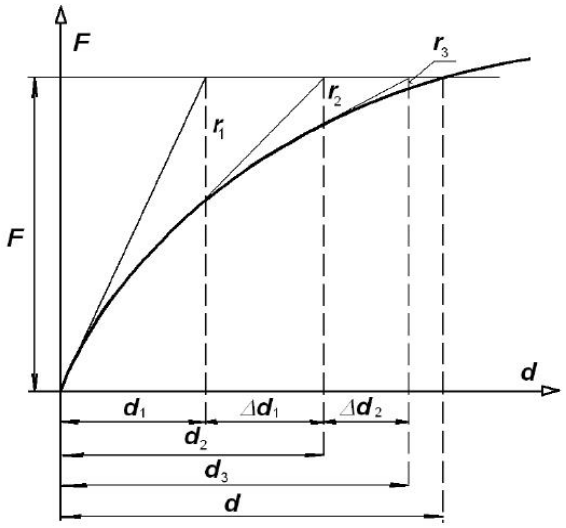

Fig. 9 Newton-Raphson method

$$\mathbb{A}_{e=1}^{n_{el}}\left(\mathbf{K}_{eff,n+1}^{(e),(i)}\Delta\mathbf{d}_{n+1}^{(e),(i)}\right)=\mathbb{A}_{e=1}^{n_{el}}\mathbf{r}_{eff,n+1}^{(e),(i)} \tag{97}$$

The effective stiffness matrix and effective residual of element are respectively defined by

$$\mathbf{K}_{eff,n+1}^{(e),(i)}=\widehat{\mathbf{K}}_{n+1}^{(e),(i)}-\mathbf{F}_{n+1}^{(e),(i)}\left(\mathbf{H}_{n+1}^{(e),(i)}\right)^{-1}\mathbf{F}_{n+1}^{(e),(i),T} \tag{98}$$

$$\mathbf{r}_{eff,n+1}^{(e),(i)}=\mathbf{r}_{n+1}^{(e),(i)}-\mathbf{F}_{n+1}^{(e),(i)}\left(\mathbf{H}_{n+1}^{(e),(i)}\right)^{-1}\mathbf{h}_{n+1}^{(e),(i)} \tag{99}$$

5. Numerical simulations

5.1 Quasi-brittle case

For both plasticity-softening model and damage-softening model, we carry out numerical analysis of a bar of a unit cross-sectional area subjected to constant velocity v = 15 m/s applied at both ends in the outward direction. The geometric and material properties of the bar are L = 2 m, E = 10000 MPa, K_s = -2500 Mpa, $\rho = 1\,\mathrm{kg/m^3}$, $\sigma_f = 900$ MPa, $\sigma_u = 880$ MPa, $\beta = 10$. The numerical results are compared for $t = \frac{1.5L}{c_e} = 0.03\mathrm{s}$ with analytical results of the strain-sofening solution presented in Section 3. In addition, results obtained from plasticity-softening model and damage-softening model will be also compared together. At this time, the bar area defined by $-\frac{L}{2} \le x \le \frac{L}{2}$ is governed by the strain-softening solution. The rest of the bar, $-L \le x < \frac{L}{2}$ and $\frac{L}{2} < x \le L$ still remains in the elastic regime. It is very obvious that the numerical results agree quite well with the predicted strain-softening behavior from exact solution wherein a displacement jump occurs and strain is supposed to be infinite in the strain-softening discontinuity at infinitesimal area near x = 0. Outside this area the bar unloads, all displacements accumulate at x = 0, and strain gradually reduces to zero. Namely, the strain-softening area narrows with increasing the number of elements and accumulation in one element of all displacements (see Figs. 10(a)-11(a)) can be observed.

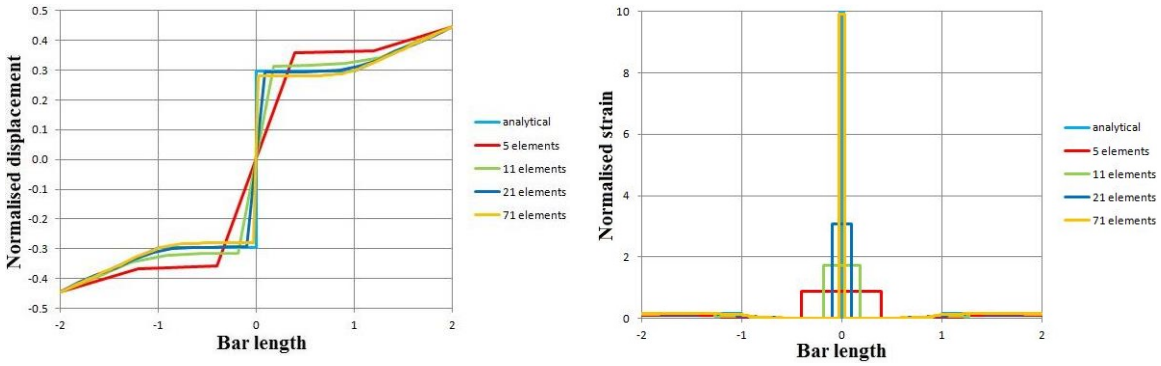

(a) Longitudinal displacement (b) Longitudinal strain

Fig. 10 Comparison between analytical and numerical solution at t = 0.03s and $\frac{\varepsilon_p}{2} < \varepsilon \le \varepsilon_p$ for plasticity-softening model

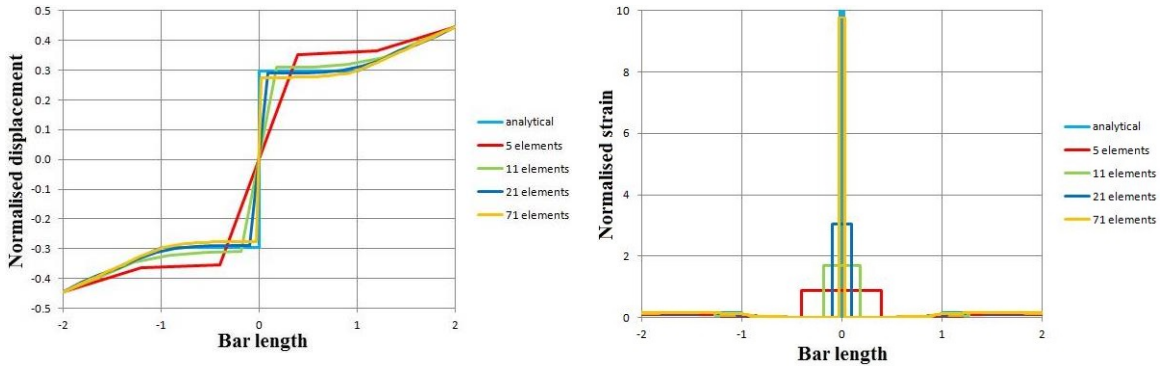

(a) Longitudinal displacement (b) Longitudinal strain

Fig. 11 Comparison between analytical and numerical solution at t = 0.03s and $\frac{\varepsilon_p}{2} < \varepsilon \leq \varepsilon_p$ for damage-softening model

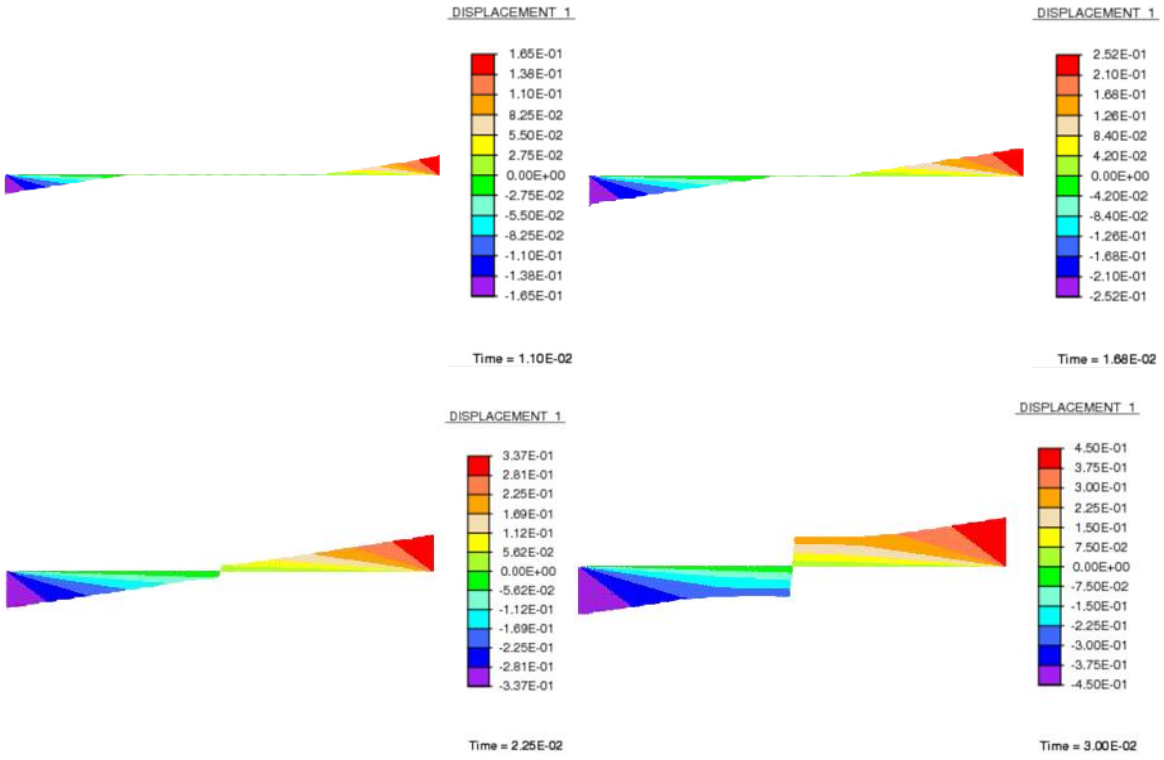

Fig. 12 Wave propagation from the right and left end to the center of the bar at different instants in time

The strain-softening element in the middle of the bar undergoes intense deformation. Strain increases with increasing mesh refinement. Strain in elements outside the strain-softening element gradually decreases to zero (see Figs. 10(b)-11(b)). Furthermore, results for longitudinal displacement and strain along the bar, respectively, in Figs. 10(a)-11(a) and Figs. 10(b)-11(b) exhibit a strong sensitivity of results on the mesh discretisation for the strain-softening zone, whereas in the remaining elastic domain mesh sensitivity is not visible although an improvement in result accuracy can be seen with increasing mesh refinement. The process in which the two step waves from the right and left boundary travel to the center of the bar in Fig. 12 indicates strain-softening behavior as expected with a displacement jump around an area of $x = 0$. Fig. 13 illustrates typical stress-strain curve for quasi-brittle case in which after reaching ultimate stress the stress-strain diagram "turns down" and material strain softens. A comparison in Figs. 14 and 15 also shows a good agreement between two models: plasticity-softening and damage-softening.

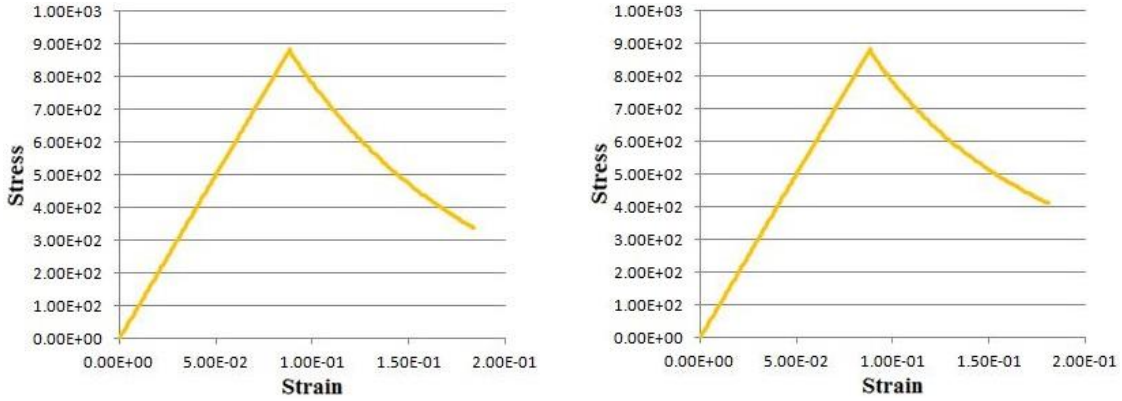

(a) Plasticity-softening model (b) Damage-softening model

Fig. 13 Typical stress-strain curve for quasi-brittle case

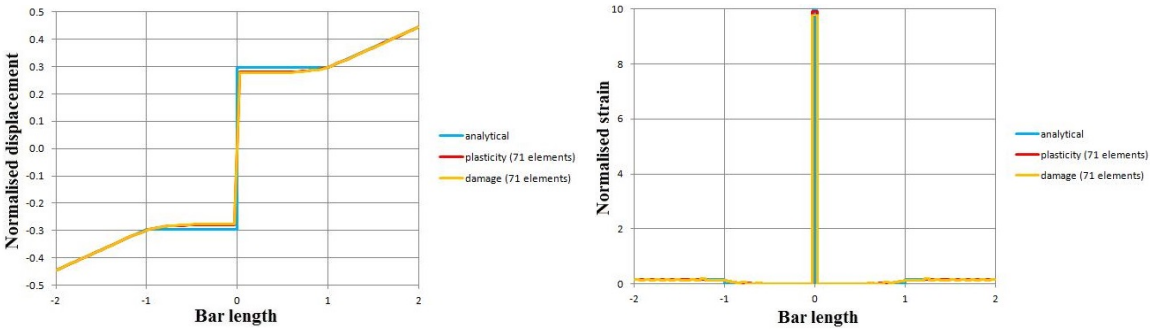

(a) Longitudinal displacement (b) Longitudinal strain

Fig. 14 Comparison between plasticity-softening model and damage-softening model.

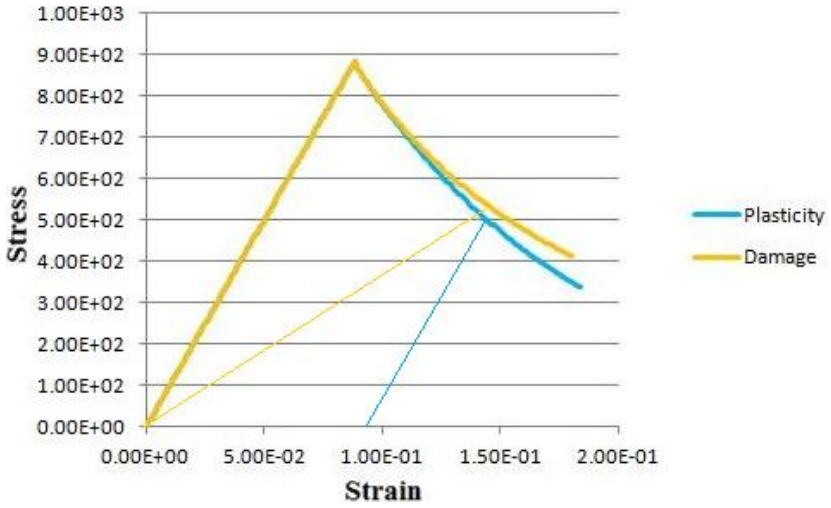

Fig. 15 Comparison between plasticity-softening model and damage-softening model

5.2 Quasi-ductile case

In the same manner, numerical analysis of a bar of unit cross-sectional area subjected to constant velocity v = 15 m/s applied at both ends in the outward direction was performed for both two models: plastitcity-softening and damage-softening. The bar has the geometric and material parameters as follows: L = 2 m, E = 10000 MPa, K = 5000 MPa, K_s = -2500 MPa, $\rho = 1\ \mathrm{kg/m^3}$, $\sigma_f = 680$ MPa, $\sigma_u = 880$ MPa, $\beta = 10$. Besides, to observe influence of ductility on failure process of material, fixed values of Young's modulus (E = 10000 MPa) and softening modulus (K_s = -2500 MPa) together with various values of isotropic hardening modulus K were used. All numerical results of different mesh discretisations are compared for $t = \frac{1.5L}{c_e} = 0.03\mathrm{s}$ with exact solution. Results obtained from plasticity-softening model and damage-softening model will also be compared together in this case. At this time ($t = \frac{1.5L}{c_e}$) the waves from the left and right have both travelled 3/2 of the bar. Consequently, the bar area defined by $-\frac{L}{2} \le x \le \frac{L}{2}$ is governed by strain-softening regime, whereas the rest of the bar obeys the elastic solution. Nevertheless, unlike quasi-brittle case, herein apart elastic and strain-softening regime material undergoes a phase of strain-hardening before failure as demonstrated in Fig. 19. Concurrently, results in Fig. 19 also allow us to confirm that the higher ductility (the smaller isotropic hardening modulus K) the larger plastic deformation material will undergo before failure and, therefore, this also implies the larger area under the stress-strain diagram, i.e., the larger strain energy density at rupture (modulus of toughness). Accordingly, the material has higher resistance to cracks and crack propagation and is more resistant to fracture. These above characteristics hold for ductile failure regime of material.

Similar to quasi-brittle case, in the case of quasi-ductile, the numerical results agree well with the predicted strain-softening behavior from the analytical point of view as aforementioned. For

more clarity, seeing results in Figs.16 and 17 where results for longitudinal displacement and strain along the bar are indicated. Moreover, propagation of waves from the both ends to the bar's center presented in Fig. 18 is well compatible with these predictions. Also, a strong sensitivity to the size of finite elements can be found in the strain-softening region, but is not present in the rest of the bar where elastic regime remains (see Figs. 16 and 17).

Finally, results obtained from damage-softening have a negligible difference in comparison with those of plasticity-softening model, and this is very clearly expressed in Figs. 20 and 21.

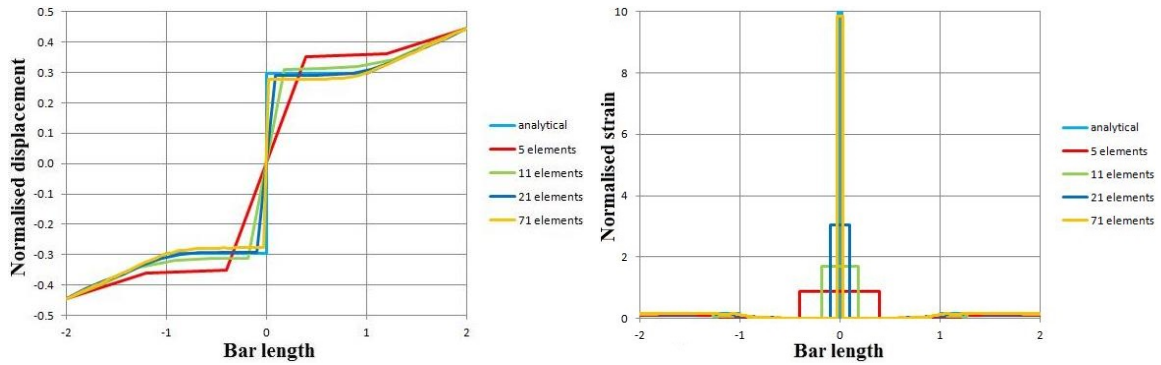

(a) Longitudinal displacement (b) Longitudinal strain

Fig. 16 Comparison between analytical and numerical solution at t = 0.03s and $\frac{\varepsilon_p}{2} < \varepsilon \leq \varepsilon_p$ for plasticity-softening model

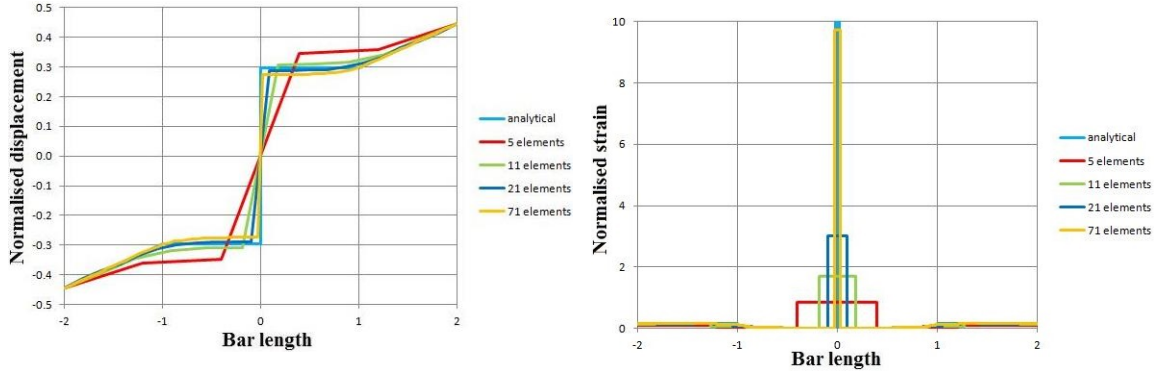

(a) Longitudinal displacement (b) Longitudinal strain

Fig. 17 Comparison between analytical and numerical solution at t = 0.03s and $\frac{\varepsilon_p}{2} < \varepsilon \leq \varepsilon_p$ for damage-softening model

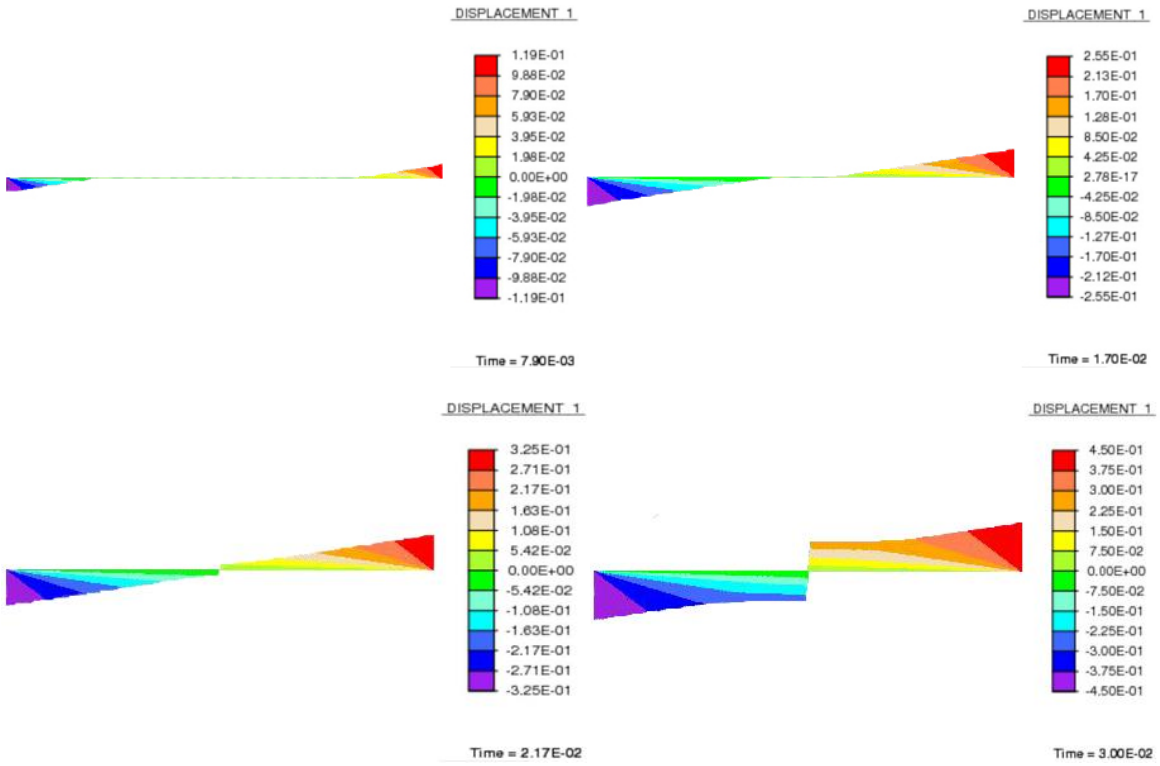

Fig. 18 Wave propagation from the right and left end to the center of the bar at different instants in time

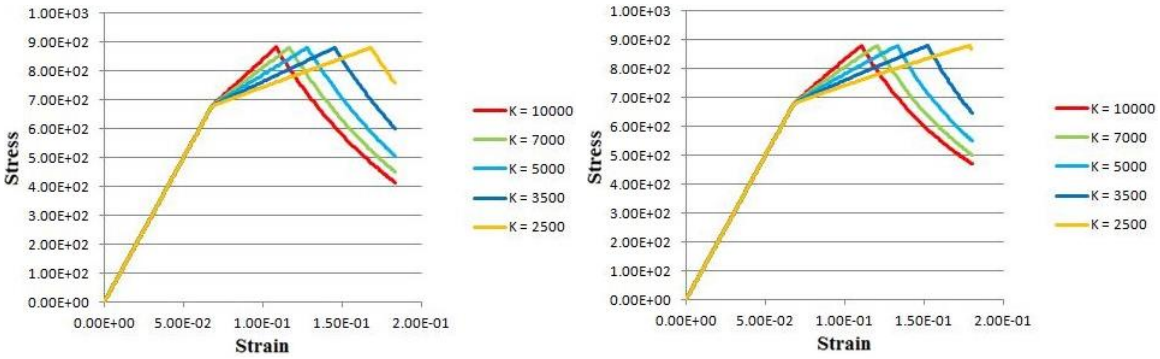

(a) Plasticity-softening model (b) Damage-softening model

Fig. 19 Typical stress-strain curve for quasi-ductile case

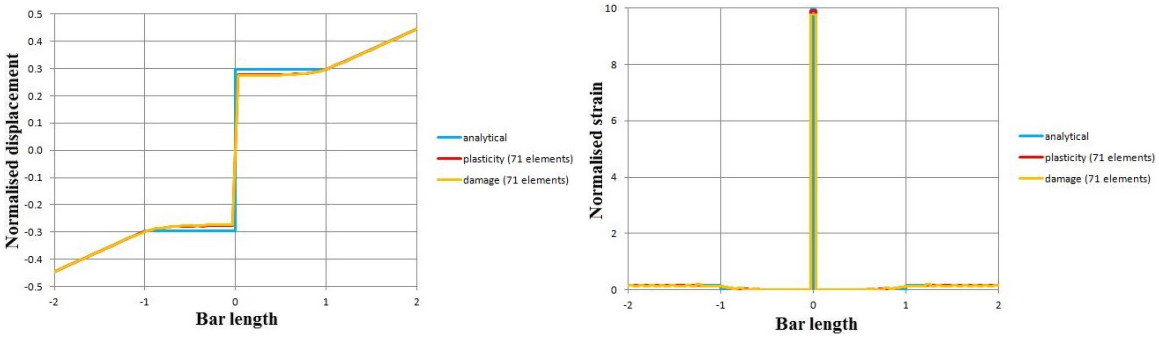

(a) Longitudinal displacement (b) Longitudinal strain

Fig. 20 Comparison between plasticity-softening model and damage-softening model

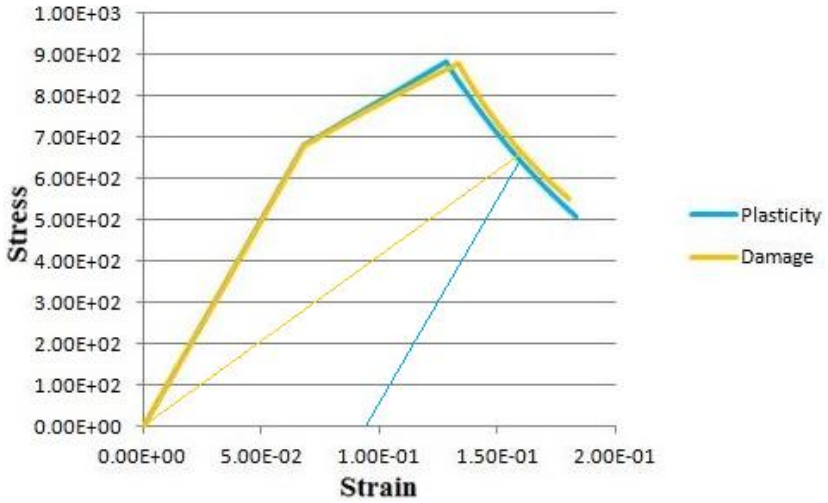

Fig. 21 Comparison between plasticity-softening model and damage-softening model

6. Conclusions

This paper contributes to enhance the understanding of localized failure both for a simple case without fracture process zone - FPZ and more general case where strain-hardening and strain-softening elastodamage behavior are combined in dynamics.

The implementation of the dynamic strain-softening problem was done with a discrete bar model with strong discontinuities in FEAP. These discontinuities are embedded into the finite element through the proper enhancement of the discrete strain field of the element. It was shown that the strain-softening area which tends to narrow with increasing mesh refinement will cause pathological sensitivity of the numerical results to the size of finite elements and all displacements accumulate in one element. Strain increases in the softening domain with a simultaneous decrease

of stress. The numerical solution compares quite well with the analytical solution with increasing number of elements. Comparison results obtained from plasticity-softening model and damage-softening model shows a very small difference.

Acknowledgments

This work was supported by the excellence scholarship from Vietnamese Ministry of Education and Training and funding of Chaire de Mécanique Picardie. This financial support is gratefully acknowledged.

References

Alfaiate, J., Wells, G.N., Sluys, L.J. (2002), "On the use of embedded discontinuity elements with crack path continuity for mode-I and mixed-mode fracture", *Eng. Fract. Mech.*, **69**(6), 661-686.

Armero, F. and Linder, C. (2009), "Numerical simulation of dynamic fracture using finite elements with embedded discontinuities", *Int. J. Fracture*, **160**(2), 119-141.

Bazant, Z.P. (1976), "Instability, ductility, and size effect in strain-softening concrete", *J. Eng. Mech. Div.*, **102**, 331-344.

Bazant, Z.P. and Belytschko, T.B. (1985), "Wave propagation in a strain-softening bar: Exact solution", *J. Eng. Mech. - ASCE*, **111**(3), 381-389.

Brancherie, D. and Ibrahimbegovic, A. (2009), "Novel anisotropic continuum-discrete damage model capable of representing localized failure of massive structures: Part I: theoretical formulation and numerical implementation", *Eng. Computations*, **26**(1-2), 100-127.

Do, X.N., Ibrahimbegovic, A. and Brancherie, D. (2015), "Combined hardening and localized failure with softening plasticity in dynamics", *Coupled Syst. Mech.*, **4**(2), 1-22.

Huespe, A.E., Oliver, J., Sanchez, P.J., Blanco, S. and Sonzogni, V. (2006), "Strong discontinuity approach in dynamic fracture simulations", *Mecánica Computacional*, **25**, 1997-2018.

Ibrahimbegovic, A. (2009), *Nonlinear Solid Mechanics: Theoretical Formulations and Finite Element Solution Methods*, Springer, Berlin, Germany.

Ibrahimbegovic, A. and Brancherie, D. (2003), "Combined hardening and softening constitutive model of plasticity: precursor to shear slip line failure", *Comput. Mech.*, **31**(1-2), 88-100.

Ibrahimbegovic, A., Hajdo, E. and Dolarevic, S. (2013), "Linear instability or buckling problems for mechanical and coupled thermomechanical extreme conditions", *Coupled Syst. Mech.*, **2**(4), 349-374.

Ibrahimbegovic, A. and Melnyk, S. (2007), "Embedded discontinuity finite element method for modeling of localized failure in heterogeneous materials with structured mesh: an alternative to extended finite element method", *Comput. Mech.*, **40**(1), 149-155.

Kachonov, L.M. (1958), "Time of the rupture process under creep conditions", *Izv. Akad. Nauk USSR Otd. Tech.*, **8**, 26-31.

Ngo, V.M., Ibrahimbegovic, A. and Hajdo, E. (2014), "Nonlinear instability problems including localized plastic failure and large deformations for extreme thermomechanical load", *Coupled Syst. Mech.*, **3**(1), 89-110.

Oliver, J. (1996), "Modelling strong discontinuities in solid mechanics via strain softening constitutive equations. Part 2: numerical simulation", *Int. J. Numer. Meth. Eng.*, **39**(21), 3601-3623.

Simo, J.C., Oliver, J. and Armero, F. (1993), "An analysis of strong discontinuities induced by strain-softening in rate-independent inelastic solids", *Comput. Mech.*, **12**(5), 277-296.

Taylor, R., *FEAP Finite Element Analysis Program*, University of California: Berkeley. (Available from http://www.ce.berkeley.edurlt).

Wells, G.N. and Sluys, L.J. (2000), "A new method for modeling cohesive cracks using finite elements. *Int. J. Numer. Meth. Eng.*, **50**(12), 2667-2682.